# 5 Noncollinear Magnetism in Systems with Relativistic Interactions

L. Sandratskii

## 5.1 Introduction

In recent years, noncollinear magnetism has attracted constantly increasing interest from the density-functional-theory (DFT) community (see, e.g. [1–19]). These studies revealed a crucial role played by noncollinear magnetism in understanding the ground state magnetic properties, excitations, transport properties, and spin-dynamics in various magnetic systems. In the present chapter, we mainly focus on one aspect of the physics of noncollinear magnetism: the interplay between the symmetry of a magnetic system, relativistic interactions and magnetic structure. The importance of the relativistic interactions in physics of magnetism clearly follows from the fact that the magnetocrystalline anisotropy, one of the properties most important for applications, and the orbital magnetism in solids are consequences of the spin-orbit coupling. Analysis of the symmetry properties allows us to make predictions important for understanding the physics of the system.

## 5.2 Density Functional Theory
of a Noncollinear Magnet

In an early formulation of the DFT by von Barth and Hedin [20], the energy of the system is treated as a functional of the two-by-two density matrix. Correspondingly, the Kohn-Sham equation (KSE) and the effective electron potential have matrix form. The consequent consideration of the matrix character of the density and effective potential allows the DFT description of systems with noncollinear magnetization. However, for many years the concrete calculations were performed for collinear magnetic systems only. In this case the density and potential matrices are assumed to have a diagonal form. In the problems where the SOC is not taken into account, the neglect of the off-diagonal elements of the potential matrix leads to the spin-factorization of the problem: the spin projection of the electron states on the global $z$-axis is a good quantum number and there are two separate equations for the electron states with opposite spin projections. Such states being used to calculate new density and potential matrices lead automatically to vanishing off-diagonal elements. Thus, if the SOC is negligible, the collinearity of

the magnetization is reproduced in the DFT calculations. In this sense, the states with collinear magnetization are always self-reproducible and can be considered as a possible ground state of a nonrelativistic system.

In the relativistic case, the neglect of the off-diagonal elements of the potential matrix does not lead to the spin-factorization of the problem because the SOC does not commute with the operator of spin projection. Therefore, the matrix form of the KSE cannot be reduced to two separate equations for the states with two opposite spin projections. The electron states have a general spinor form

$$\psi(r) = \begin{pmatrix} \psi_1(r) \\ \psi_2(r) \end{pmatrix},$$

and the direction of the magnetization corresponding to these states varies from point to point.

Physically, it is useful to distinguish between *interatomic* and *intraatomic* magnetic noncollinearities. Under interatomic noncollinearity we understand the noncollinearity of the atomic magnetic moments obtained by the integration of the magnetization over the atomic volumes. On the other hand, the intraatomic magnetic noncollinearity is the noncollinearity of the magnetization within the volume of a given atom.

Since the relativistic KSE always has a matrix form, the intraatomic magnetization of a relativistic system is always noncollinear [4]. The intraatomic magnetic noncollinearity of relativistic systems does not necessary lead to the noncollinearity of the moments of different atoms. If the intraatomic exchange interaction is stronger than the SOC, the neglect of the intraatomic noncollinearity of a relativistic system is a good approximation [21]. In this chapter we will mostly be interested in the aspects of the interatomic noncollinearity.

The calculational scheme used in the main body of the calculations discussed in this chapter is described in [11,22,23]. An important feature of this scheme is an allowed variation of the directions of the atomic moments from iteration to iteration: The eigenstates of the Kohn-Sham Hamiltonian (KSH), $\psi$, are used to calculate the density matrix

$$\rho(r) = \sum_{i,occ} \psi_i(r)\psi_i^\dagger(r).$$  (5.1)

After integration of (5.1) over atomic spheres one gets the atomic matrices [22]. Diagonalization of the atomic matrices gives the directions of the atomic magnetic moments corresponding to these matrices. In general, calculated directions of the atomic moments are different from the directions used in the formulation of the KSH at the beginning of the iteration. In the self-consistent state, the initial and calculated directions of atomic moments coincide. If the intraatomic noncollinearity of the spin magnetization is taken

into account, the condition of self-consistency is imposed on the magnetic density. According to the basic theorems of the DFT the ground magnetic state corresponds to a self-consistent magnetic density [20].

## 5.3  Relation Between Symmetry and Stability of Magnetic Structures

The relation between the symmetry of a system and its magnetic structure has attracted much attention in the history of solid-state magnetism. Much consideration was given to the prediction of the magnetic structures that can appear in the system as the result of a continuous phase transition (see, e.g. [24,25]). We will focus on another aspect of the relation between the symmetry and magnetic structure: the stability of a given magnetic configuration, independent of the kind of phase transition into the magnetic state. Applications of the DFT to the studies of complex noncollinear magnetic configurations have shown that the magnetic structure chosen at the beginning of the DFT calculation is, in general, unstable: the magnetic moments deviate in the course of iterations from the initial directions, tending to form another magnetic state. On the other hand, in some cases the magnetic moments, although allowed to move, keep their initial directions. The ability to predict to which of the two types of structures a given magnetic configuration belongs is an important capability for the study of the magnetism of the system.

In [3,11,26,27] it was shown that there exists an intimate connection between the stability of the magnetic structure in the DFT calculations and the symmetry of the system. Here, we will generalize the approach suggested in [3,11,26,27] by using the notion of symmetry constraint and apply it to the studies of the properties of various magnetic structures.

### 5.3.1  Symmetry Constraint: General Formulation

We begin with the proof of the statement that the symmetry of the initial Kohn-Sham Hamiltonian is preserved in the iterational DFT calculations. Let us assume that the initial KSH of the problem commutes with the operators of group G and show that the density matrix, obtained with the use of the solutions of the Kohn-Sham equation, is invariant with respect to the operators of G. The concrete form of the KSH is not important here. For nonrelativistic problems the operations are of the $\{\alpha_S|\alpha_R|t\}$ type where $\alpha_S$ is a spin rotation, $\alpha_R$ is a space rotation, $t$ is a space translation [11]. (In this chapter we do not distinguish between nonrelativistic and scalar-relativistic cases, since from the symmetry viewpoint they are equivalent.) In the case of relativistic problems $\alpha_S$ is always equal to $\alpha_R$ and the operators are of the $\{\alpha_R|\alpha_R|t\} \equiv \{\alpha_R|t\}$ type [11,28]. In both cases these transformations can be accompanied by time reversal.

According to the basic theorems of quantum mechanics, if operator $\hat{g}$ commutes with Hamiltonian $\hat{H}$ and $\psi$ is an eigenfunction of $\hat{H}$ corresponding to eigenvalue $\varepsilon$, then $\hat{g}\psi$ is also an eigenfunction corresponding to the same energy. As a consequence, all eigenstates of $\hat{H}$ can be separated into the subsets such that the states of one subset correspond to the same energy and form a basis of an irreducible representation of $G$. The contribution to the density matrix (5.1) of any such subset is invariant with respect to the operations of $G$. Indeed,

$$\hat{g}\sum_{\nu}\psi_{\nu}^{j}(r)\psi_{\nu}^{j\dagger}(r) = \sum_{\nu}\hat{g}\psi_{\nu}^{j}(r)(\hat{g}\psi_{\nu}^{j}(r))^{\dagger} \tag{5.2}$$

$$= \sum_{\nu}\sum_{\mu}D_{\mu\nu}^{j}(\hat{g})\psi_{\mu}^{j}(r)\sum_{\eta}D_{\eta\nu}^{j*}(\hat{g})\psi_{\eta}^{j}(r))$$

$$= \sum_{\mu\eta}(\sum_{\nu}D_{\mu\nu}^{j}(\hat{g})D_{\eta\nu}^{j*}(\hat{g}))\psi_{\mu}^{j}\psi_{\eta}^{j} = \sum_{\nu}\psi_{\nu}^{j}(r)\psi_{\nu}^{j\dagger}(r).$$

Here $D^{j}$ is the $j$th irreducible representation of $G$.

Since

$$\rho(r) = \frac{1}{2}\begin{pmatrix} n(r)+m_{z}(r) & -im_{x}(r)+m_{y}(r) \\ im_{x}(r)+m_{y}(r) & n(r)-m_{z}(r) \end{pmatrix}, \tag{5.3}$$

the invariance of the $\rho$ matrix immediately means the invariance of the particle density $n$ and spin magnetic density $m$ with respect to $\hat{g}$. Therefore the effective potential

$$v(r) = v_{o}[n(r)] + \Delta v[n(r),m(r)]\,\sigma\cdot\frac{m(r)}{|m(r)|}, \tag{5.4}$$

calculated with the use of densities $n$ and $m$ is also invariant with respect to $\hat{g}$. As a result, the KSH for the next iteration, which uses the calculated effective potential (5.4), is again, as the initial one, invariant with respect to operations of $G$.

Thus we have shown that the densities obtained in the calculations are invariant with respect to the symmetry operations of the initial KSH and any symmetry operation of the initial KSH is preserved in the calculations. Since only the densities invariant with respect to operations of $G$ appear in the calculations, one deals with a constrained minimization of the total energy considered as a functional of the densities. We will refer to this type of restrictions on the densities as symmetry constraint.

A general approach to a constrained minimization of the energy as a functional [29,30] of the charge and magnetic densities requires adding to the functional the following term

$$\int dr(p(r)(\hat{g}n(r) - n(r)) + b(r)(\hat{g}m(r) - m(r)).$$

This term contains Lagrange parameters $p(r)$ and $b(r)$, which play the role of external fields stabilizing the constrained state.

A remarkable feature of the symmetry constraint is that the state providing the minimum of the functional under the symmetry restriction does not need a nonzero stabilizing external field. This follows from the property that the symmetry of the KSH and densities is preserved in calculations.

The property that a symmetry-constrained state does not need an external stabilizing field is of exceptional importance since only such states can be the ground state of the system. This property permits cardinal simplification of the calculation of the ground state if the experimental data and theoretical considerations show the presence of certain symmetry in the system. Note, that the DFT allows, in principle, to begin calculations with a random magnetization and, by carrying out the iterational process to self-consistency, to determine the magnetic state with the minimal energy. A highly symmetrical ground state can be established in such calculations since, opposite to the loss of symmetry, an increase of symmetry in the DFT calculations is possible. These calculations are, however, extremely complex and time consuming even for the simplest magnetic systems. Therefore, the symmetry constraint is an efficient tool in the DFT studies of magnetic systems.

### 5.3.2 Two Types of Symmetry Constraints

We will distinguish two types of symmetry constraints. To introduce them we consider in more detail the restrictions imposed on the magnetization by the condition that the magnetization is invariant with respect to the operations of group $G$.

Since, on the one hand, the symmetry operation $\hat{g}$ transforms the magnetic density $m(r)$ and, on the other hand, leaves it invariant, the magnetization must fulfil the following condition [53]

$$\{\alpha_{S}|\alpha_{R}|t\}m(r) \equiv \alpha_{S}m(\{\alpha_{R}|t\}^{-1}r) = m(r). \tag{5.5}$$

After integration of the magnetization over atomic spheres we get the restriction

$$m_{i} = \alpha_{S}m_{j}, \tag{5.6}$$

imposed on the atomic magnetic moments, where $i$ and $j$ label the atoms defined by the relation

$$\{\alpha_{R}|t\}a_{i} = a_{j}. \tag{5.7}$$

Therefore the atoms that are transformed one into another by $\hat{g}$ possess magnetic moments of equal magnitude, and the direction of one moment is transformed into the direction of another under the action of $\hat{g}$. In the case when the position of an atom is unchanged under the action of $\hat{g}$, (5.6) takes the form

$$m_{i} = \alpha_{S}m_{i},$$

**(a)** **(b)**

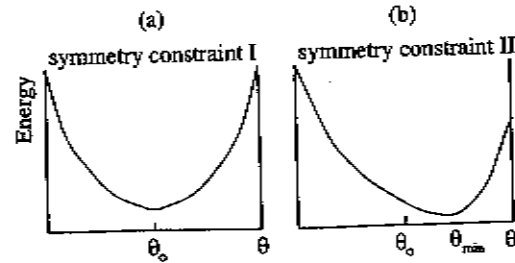symmetry constraint I   symmetry constraint II



**Fig. 5.1.** Symmetry constraints I and II (schematic picture). The continuous parameter $\theta$ describes different magnetic configurations. (a) The state with $\theta = \theta_0$ corresponds to the symmetry constraint I. This state possesses additional regular features compared with the states with $\theta \neq \theta_0$ (b) Symmetry constraint II. The states with different $\theta$ possess the same regular features. The probability that $\theta_0$ accidentally coincides with $\theta_{min}$ is negligible

and imposes a restriction on the moment of this atom, which consists of the invariance of the moment with respect to $\hat{g}$. If operation $\hat{g}$ contains time reversal, (5.6) is modified as follows

$$m_i = -\alpha_g m_j.$$

(5.8)

The restrictions (5.6–5.8) on the lengths and directions of the atomic magnetic moments can be considered as regular features (regularities) of the magnetic structure that are the necessary consequences of a given symmetry constraint. Two different situations can follow from relations (5.6–5.8). In the first case, the symmetry constraint determines the magnetic structure uniquely. This means that any deviation of the magnetic moments from the initial directions disturbs, at least, one of the symmetry operations. Since all symmetry operations must be preserved the structure cannot change in the course of calculations. We will refer to this type of constraint as symmetry constraint I (Fig. 5.1).

In the second case (symmetry constraint II) there is an infinite set of magnetic configurations that, first, satisfy the conditions (5.6–5.8) imposed by the invariance with respect to $G$ and, second, can be continuously transformed into one another without disturbing the symmetry of the system. Let $\theta$ be a continuous parameter that describes this set of magnetic configurations. (The number of parameters can be larger than one, but this does not change the essence of the arguments.) As all magnetic configurations are described the same symmetry none of the $\theta$ values is distinguished. The purpose of the DFT calculations in this case is to find the value of $\theta$ that corresponds to the state with the lowest energy. Since all $\theta$ values are equivalent, this minimum cannot be predicted without calculations (Fig. 5.1).

To begin the DFT calculation a value $\theta_0$ of parameter $\theta$ is selected. Since it is improbable that $\theta_0$ accidentally equals $\theta_{min}$, providing the minimum of

the total energy, the initial state in the case of symmetry constraint II is unstable. In the iterational process, the magnetic structure deviates from the state described by $\theta_0$ tending to assume the state with the lowest energy. Note that a self-consistent DFT calculation for the state with arbitrary $\theta$ is possible. This calculation needs, however, an additional (nonsymmetry) constraint on the system [29]. This additional constraint requires application of an external stabilizing field.

The situation described by symmetry constraint II is related to many interesting physical phenomena. In a typical case, the neglect of a part of the interactions leads to the ground state of the system that belongs to constraint I and, therefore is uniquely determined by symmetry. With account for the full Hamiltonian this state corresponds, however, to symmetry constraint II. Therefore, in the full-Hamiltonian study it becomes unstable and a variation of the state must take place. Examples of such systems are, e.g. $Fe_2O_3$ and $Mn_3Sn$, where the SOC leads to the phenomenon of weak ferromagnetism [11].

Summarizing this section we can formulate a number of conclusions. First, a given magnetic structure is stable in the DFT calculations only in the case when it corresponds to symmetry constraint I. Second, if the structure corresponds to symmetry constraint II its variation is subjected to restrictions imposed by the relations (5.6–5.8). Thus, although the structure itself is unstable, the regularities in the magnetic state that follow from (5.6–5.8) are preserved features of the magnetic structure. On the other hand, an assumed regularity in the initial magnetic structure that is not supported by a symmetry operation is not a stable feature of the magnetic state of the system.

It is important to distinguish between the stability in the DFT calculations and the stability in the nature. Magnetic configurations stable in the calculations may not necessarily be the physical ground state, since random fluctuations characteristic of real systems are absent in the DFT calculations. Therefore the symmetry constraint is not efficient in the real systems. On the other hand, the instability of a magnetic state in the DFT calculations can be directly related to the instability in nature, because this instability is a consequence of the interactions in the system. The latter property is of primary importance for the discussion of concrete physical systems in the next section. In the next sections we apply the symmetry principles to the analysis of various magnetic systems.

## 5.4 Stable Magnetic Structures

First, we consider examples of magnetic structures distinguished by symmetry relative to the structures obtained by infinitesimal variation of the directions of atomic moments.

### 5.4.1  Simple Standard Cases

With rare exceptions, the DFT calculations reported in the literature are performed under a symmetry constraint. Historically, the first calculations were carried out for the nonmagnetic state of the systems. The magnetic density was assumed to be zero at each point in the space. The study of magnetically ordered systems began with the collinear ferromagnetism of elementary metals, like Fe and Ni, and of the two-sublattice collinear antiferromagnetism of Cr [31].

It can be easily shown that the regularities characteristic to all three simplest magnetic states correspond to the symmetry constraint and, indeed, must be stable in the calculations. The stability of the zero value of the magnetic moments in the nonmagnetic state is a consequence of the invariance of the KSH with respect to the time reversal. The stability of the equal values and parallel directions of the atomic moments in Fe and Ni are the consequences of the translational symmetry. The stability of the equal values and antiparallel directions of the magnetic moments of two sublattices in Cr are the consequence of the symmetry operation that combines a lattice translation connecting two sublattices and the time reversal. Any disturbance of the characteristic features of these magnetic states leads to the loss of the invariance of the KSH with respect to the corresponding symmetry operation.

### 5.4.2  Magnetic Structures of $U_2Pd_2Sn$ and USb

The crystallographic unit cell of the $U_2Pd_2Sn$ compound is shown in Fig. 5.2. The magnetic state of $U_2Pd_2Sn$ was established in [32] where six magnetic structures, shown schematically in Fig. 5.2, were considered in the analysis of the neutron diffraction data. These six structures were selected on the basis of the symmetry arguments of the Landau theory of the second-order phase transitions. The noncollinear magnetic configuration NC1 was found to be the magnetic ground state of the system.

We performed the first-principles DFT calculations for all six magnetic configurations. All of them correspond to the symmetry constraint I and are stable in the calculations. For example, the magnetic structure NC1 possesses the following symmetry operations: (a) the 180° rotation about the $z$-axis, (b) the 180° rotation about the $x = y$-axis, (c) the 90° rotation about the $z$-axis accompanied by inversion, (d) the 90° rotation about the $z$-axis accompanied by time reversal. (Only the generators of the symmetry group are given.) If the coordinate center is chosen at the position of the central Sn atom (Fig. 5.2) operation (b) is accompanied by nonprimitive translation $a(0.5, 0.5, 0)$. Other operations are pure point transformations. Any infinitesimal deviation of the system with respect to at magnetic moments destroy the invariance of the system with respect to at least one of the symmetry operations. This additional symmetry of the NC1 structure is illustrated in Fig. 5.3, where we show the total energy of the magnetic structures obtained by the rotation of the NC1 structure by different
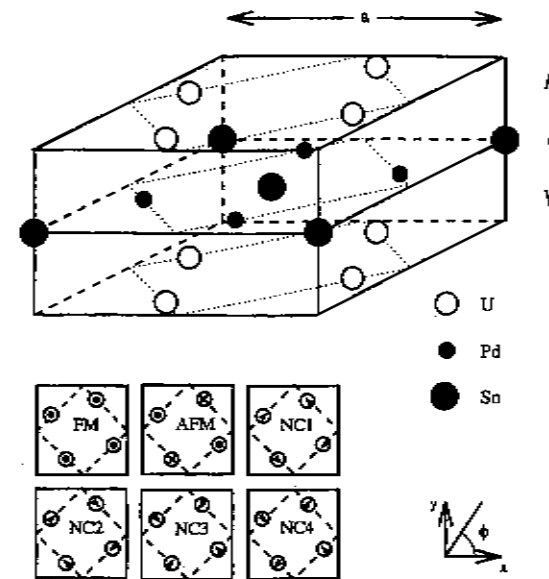
Fig. 5.2. Unit cell of the $U_2Pd_2Sn$ crystal structure. The six magnetic structures studied are indicated

angles about the $z$-axis. The structure NC1 can be transformed into NC4 by a rotation by 90° about the $z$-axis.

All structures lying between the NC1 and NC4 structures have the same symmetry and are invariant with respect to operations (a), (c), and (d). They are less symmetrical than the NC1 and NC4 configurations. This property results in the extrema of the total energy for NC1 and NC4 structures. The form of the curve shows clearly that in the case of the NC1 configuration we deal with symmetry constraint I (Fig. 5.3). Note that all intermediate magnetic states in Fig. 5.3 are unstable and the nonsymmetry constraint was used in the calculations of these states.

Another example of a stable magnetic state is a so-called triple-$k$ magnetic structure in USb (Fig. 5.4). The list of the symmetry operations of this structure can be found in [33].

In the next sections, we consider relativistic instabilities of the regular features of magnetic structures.
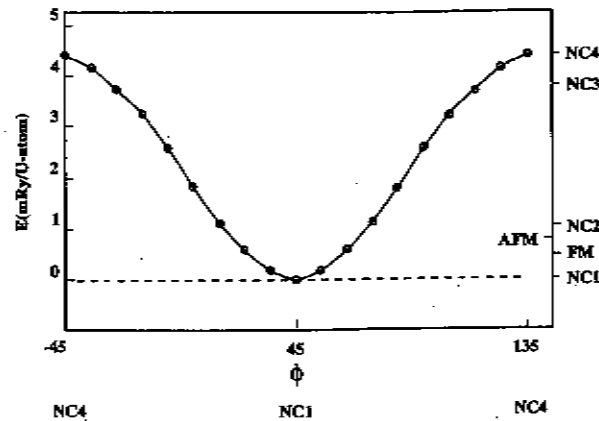
Fig. 5.3. Total energy of $U_2Pd_2Sn$ as a function of $\phi$ calculated with SOC (*solid line*) and without SOC (*dashed line*). On the *right-hand side* the energies of the six magnetic structures (see Fig. 5.2) are indicated
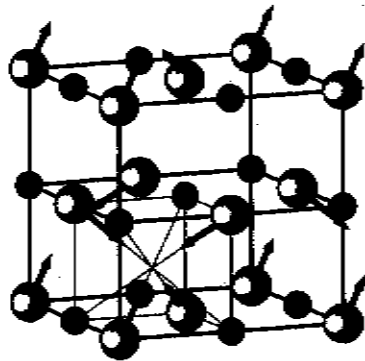


Fig. 5.4. Triple-*k* structure in USb

## 5.5    Relativistic Instability of Collinear Ferromagnetism

In nonrelativistic systems, collinear magnetic configurations are always stable in the calculations. The symmetry operations responsible for the stability of this regularity are the pure spin rotations about the magnetization axis [11]. In the relativistic case, such operations do not commute with the Hamiltonian of the problem and cannot be symmetry operations of the system. The pure spin rotations are not the only symmetry operations that can be responsi-
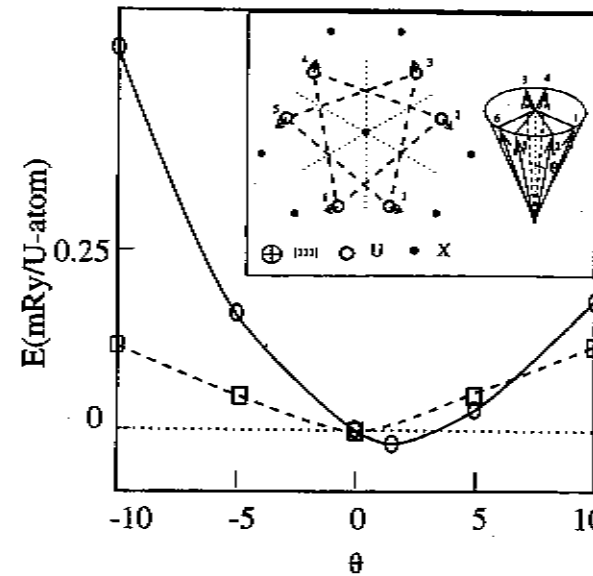
Fig. 5.5. The total energy of $U_3P_4$ as a function of the deviation of the magnetic moments from the (111) axis. *Solid/dashed line* shows the result of the calculation with/without the spin-orbit coupling. The *inset* shows the projection of the crystal and magnetic structure onto the (111) plane. The magnetic moments form a cone structure

ble for the stability of a collinear magnetic state. For example, the lattice translations and combined spin-space rotations about the axis parallel to the magnetic moments are examples of such operations. If, however, the system possesses none of the symmetry operations responsible for the stability of a collinear magnetic configuration, this structure must be unstable. Below, we consider two examples of the system with instabilities of the collinear ferromagnetic structure.

### 5.5.1    Magnetic Structure of $U_3P_4$

The inset in Fig. 5.5 shows the experimentally determined magnetic structure of $U_3P_4$. The atomic moments form a cone with the axis parallel to the (111) axis. The system possesses a strong ferromagnetic component. The DFT calculation started with all U moments parallel to the (111) axis results immediately in the noncollinear magnetic structure similar to the structure found in the experiment [3]. Analysis of the symmetry of the system shows

that the deviation of the magnetic moments does not influence the symmetry of the magnetic structure. Therefore, we deal here with symmetry constraint II and the initial collinear structure must be unstable. The minimum of the total energy is at an accidental point.

With the SOC being neglected, the curve of the total energy as a function of the deviation angle $\theta$ is symmetrical with respect to the change of the sign of $\theta$ (Fig. 5.5). Therefore, the collinear configuration corresponding to $\theta = 0$ is distinguished by symmetry and is stable [3].

### 5.5.2  Atomically Disordered Relativistic Systems

Another example of the system with relativistic instability of collinear magnetic state is an atomically disordered relativistic system. According to the symmetry principles formulated in Sect. 5.3.1 *the magnetic structure of relativistic systems with atomic disorder is always noncollinear*. Indeed, in the presence of atomic disorder there is no spatial transformations that leave the atomic positions invariant. Since the spin-orbit coupling connects the atomic and magnetic subsystems, a separate transformation of these subsystems is not allowed. Correspondingly, the system possesses no symmetry operation that can be responsible for the collinearity of the atomic moments. This leads to the noncollinearity of the magnetic structure.

To verify this conclusion, the following DFT calculations have been performed. First, undistorted bcc Fe was considered. In this case the collinear ferromagnetic structure is stable for both relativistic and nonrelativistic calculations (see Sect. 5.4.1). At the next stage, a supercell containing 8 atoms was constructed and the atoms were shifted from their positions in the bcc lattice (Fig. 5.6) by different vectors collected in Table 5.1. These shifts destroy the symmetry operations of the bcc structure that transform the atoms of the super cell into one another. As a result, there is no symmetry operation that can be responsible for the stability of the collinear directions of the magnetic moments of any two atoms in the super cell. Therefore, according to the symmetry analysis of Sect. 5.3.1 each of the 8 atomic moments must deviate from the initial direction. These deviations must be different for each of the 8 atoms.

The calculations confirmed these predictions. At the beginning, all magnetic moments were directed parallel to the z-axis (Fig. 5.6). Already the first iteration resulted in different deviations of the moments of all 8 atoms from the initial direction. The self-consistent deviation angles are collected in Table 5.1. It is important that not only the spin moments of different atoms deviate differently but also the orbital and spin moments of the same atom assume different directions. This property is another consequence of the loss of the symmetry in the system. The collinearity of the spin and orbital moments of the same atom is a regularity that can be stable only if it is supported by a symmetry operation. In the case of symmetry constraint II, the directions of the spin and orbital atomic moments are always different.
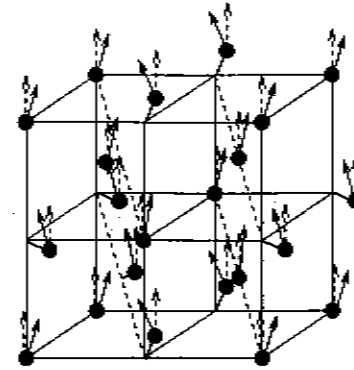
**Fig. 5.6.** Atomic disorder leads to the noncollinearity of the magnetic structure. *Broken arrows* show the initial collinear structure

**Table 5.1.** Noncollinear magnetic structure of distorted bcc iron: self-consistent relativistic calculations. Atomic positions and shifts are given in the units of the bcc lattice parameter, the deviation angles in degrees

| bcc position | shift | Deviation of atomic moments | |
|---|---|---|---|
| | | spin $\theta, \phi$ | orbital $\theta, \phi$ |
| $(0,0,0)$ | | 0.81,188.8 | 1.63,215.6 |
| $(\frac{1}{2},\frac{1}{2},\frac{1}{2})$ | $(0.01,0.02,0.03)$ | 0.79,193.6 | 0.96,206.8 |
| $(0,0,1)$ | $(0,0.01,0.01)$ | 0.69,191.1 | 0.28,78.7 |
| $(\frac{1}{2},\frac{1}{2},\frac{3}{2})$ | $(-0.02,0,-0.01)$ | 0.73,188.8 | 1.26,309.2 |
| $(0,1,0)$ | $(0,-0.03,0)$ | 0.83,193.2 | 1.37,180.4 |
| $(\frac{1}{2},\frac{3}{2},\frac{1}{2})$ | | 0.81,194.5 | 1.48,233.8 |
| $(0,1,1)$ | | 0.72,195.4 | 0.93,78.4 |
| $(\frac{1}{2},\frac{3}{2},\frac{3}{2})$ | | 0.77,189.6 | 1.04,325.8 |

## 5.6  Relativistic Instability of Collinear Antiferromagnetic Structures

Next we discuss two examples of the relativistic instability of collinear antiferromagnetic structures.

### 5.6.1  Weak Ferromagnetism in $\alpha$-$Fe_2O_3$

We begin with the phenomenon of weak ferromagnetism in hematite, $\alpha$-$Fe_2O_3$ [34]. Dzialoshinski [35] suggested a model Hamiltonian

$$H = I_{ij}S_iS_j + D_{ij} \cdot [S_i \times S_j] + S_i \cdot K_i \cdot S_i, \tag{5.9}$$

that gave a basis for most of further work on weak ferromagnetism. In (5.9) the indices $i$ and $j$ number the atoms in the lattice, $I_{ij}$ and $D_{ij}$ are the symmetric and antisymmetric exchange constants and the tensor $K_i$ contains information about the single ion magnetocrystalline anisotropy. The first term of the Hamiltonian (5.9), the symmetric exchange, is supposed to lead to a compensated magnetic configuration. The next two terms, the anisotropic exchange and the magnetocrystalline anisotropy terms, respectively, can lead to a small ferromagnetic moment in an otherwise antiferromagnetic crystal.

Moriya [36] showed that depending on the type of crystal structure either of two mechanisms, antisymmetric exchange or magnetocrystalline anisotropy, can be the origin for the canting of magnetic moments. Thus, in the case of $\alpha$-Fe$_2$O$_3$ it is the antisymmetric exchange that plays the dominant role, whereas in the case of NiF$_2$ antisymmetric exchange is ruled out in favor of the magnetocrystalline anisotropy, which here is responsible for the appearance of the ferromagnetic component.

$\alpha$-Fe$_2$O$_3$ is a classical example of the weak ferromagnetism caused by the antisymmetric exchange. The triangular antiferromagnet Mn$_3$Sn is considered in Sect. 5.7 and is a system where the antisymmetric exchange contributions from different atoms cancel and cannot be a reason for the observed weak ferromagnetism. In this case, the magnetocrystalline anisotropy term is seen to be responsible for weak ferromagnetism.

The crystal structure of Fe$_2$O$_3$ is shown in Fig. 5.7. This is a rhombohedral lattice with a basis of two formula units per unit cell. The following operations are the generators of the group characterizing the symmetry of the atomic positions: rotation by 120° about the $z$-axis, rotation by 180° about the $y$-axis, and inversion.

Calculations with the SOC neglected [37] have shown that the magnetic state with the lowest energy is a collinear antiferromagnetic structure of the type $(+ - -+)$. Here, $+$ and $-$ designate up and down directions of the Fe moments with respect to some chosen axis. This result is in agreement with experiment.

If we next choose the $z$-axis as the direction of the magnetic moments and switch on SOC, the following generators remain in the symmetry group of the Kohn-Sham Hamiltonian: rotations about the $z$-axis and the inversion [39]. The symmetry operations that are of special importance for us are the rotations about the $z$-axis: none of them change the position of any of the four Fe atoms lying on the axis of rotation. The directions of the magnetic moments are parallel to this axis and are not changed either. It is clear that any deviation of the magnetic moments from the $z$-axis will destroy the invariance of the crystal with respect to this operation. As the symmetry of the Hamiltonian cannot become lower during iterations this change is forbidden by symmetry and the magnetic structure will remain collinear during iterations even in the presence of SOC. This result agrees
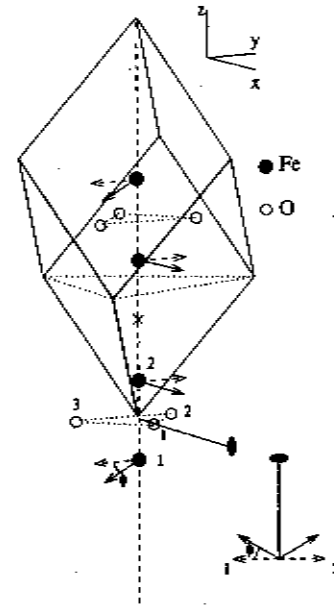
Fig. 5.7. The unit cell of Fe$_2$O$_3$. *Cross* on the diagonal of the rhombohedron shows the point of inversion. The *solid line* passing through the 1st oxygen atom indicates a two-fold symmetry axis. The collinear (*dashed arrow*) and canted (*solid arrow*) directions of the Fe atoms are shown. The canting of the Fe moments in the $xy$ plane is illustrated differently in the *lower right corner* of the figure

with the experimental observation of a collinear antiferromagnetic structure with moments oriented parallel to the $z$-axis below 260 K [38].

The situation is changed completely when the moments are parallel to the $y$-axis arranged again in the sequence $(+ - -+)$ [39]. Now the following generators are left in the symmetry group of the KSH: the 180°-rotation about the $x$-axis and the inversion. Inversion transforms the atoms of the upper Fe$_2$O$_3$ molecule into the atoms of the lower molecule, see Fig. 5.7. Since the magnetic moments are axial vectors, they do not change under this transformation. Hence, corresponding atoms of two molecules must keep parallel moments and one may restrict the consideration to the lower molecule in Fig. 5.7. The only condition imposed on the moments of the Fe atoms by symmetry is the transformation of the moment of atom 1 into the moment of atom 2 by the rotation through 180° about the $x$-axis. However, to fulfil this condition it is not necessary for the atomic moments to be parallel to the $y$-axis nor to remain collinear. Indeed, calculations show that the magnetic

moments move and deviate from their collinear directions toward the direction of the $x$-axis until an "accidental" self-consistent magnetic structure will be achieved. Since, without SOC, the magnetic structure remains collinear, the canting of the magnetic moments is a direct result of this interaction. Because of the small value of SOC compared with the exchange coupling that is responsible for the antiparallel directions of atomic moments, the canting of the moments is rather small and leads in the calculation to a ferromagnetic moment of about $0.002\,\mu_B$ per Fe atom [39]. This estimate is in quite good agreement with the experimental value.

### 5.6.2 Relativistic Instability of the Collinear Antiferromagnetism in UPdSn

Much attention was recently attracted by two magnetic phase transitions [40–44] in UPdSn. The paramagnetic state has the hexagonal GaGeLi crystal lattice. Below 45 K UPdSn becomes magnetic with a noncollinear antiferromagnetic structure. In this phase (which we will refer to as structure I) all magnetic moments of the Uranium atoms lie parallel to a plane and compensate one another completely. Simultaneously, orthorhombic lattice distortions are detected. At 20 K, a second phase transition is observed. Here, the magnetic structure (structure II) is still noncollinear and compensated, however, the magnetic moments deviate from the plane, developing components perpendicular to it.

The calculations [45] were started with the undistorted hexagonal lattice and uranium magnetic moments directed along the $z$-axis and forming a collinear antiferromagnetic structure (see Fig. 5.8a). Allowed to rotate, the moments deviated immediately from the $z$-axis keeping, however, their equivalence and the compensated character of the magnetic structure. The resulting self-consistent directions of the magnetic moments are shown in Fig. 5.8a; they form a magnetic structure that is very similar to the experimental structure I. The symmetry principle, formulated above helps us to expose the physical reasons for the instability of the initial collinear structure.

The symmetry operations of the initial collinear antiferromagnetic structure are collected in Table 5.2. The analysis of the restrictions imposed by the symmetry operations on the directions of the magnetic moments shows that $m_z^i=0$ for each atom $i$. For the other two components the following conditions must be satisfied: $m_y^1 = m_y^2 = -m_y^3 = -m_y^4$ and $m_x^1 = -m_x^2 = m_x^3 = -m_x^4$. This means that the initial collinear structure has the same symmetry as a noncollinear magnetic structure satisfying these relations. The noncollinear magnetic structure detected experimentally belongs to this type of structure. Thus, we again deal with the case of symmetry constraint II.

Next, the influence of lattice distortions on the magnetic structure was studied [45]. First, following the experiment [42] we introduced a small variation of the lattice parameters $a$ and $b$ such that the relation $b = \sqrt{3}a$, valid for the ideal hexagonal lattice, is no longer satisfied. This distortion does not
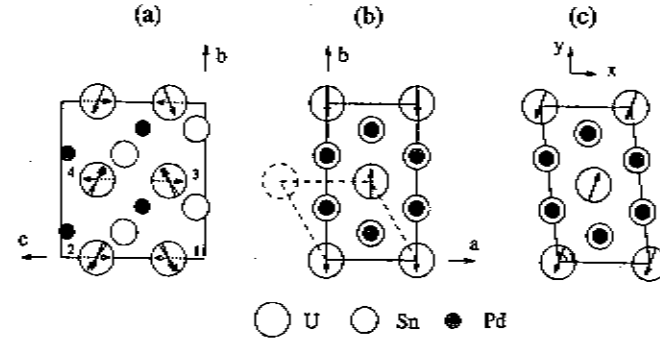
**Fig. 5.8.** Projections of the crystal and magnetic structure onto the $xy$ and $yz$ planes. (a) Projection of the orthorhombic unit cell onto the $yz$ plane. *Dotted arrows* show the initial magnetic structure used to start the calculation, *thick arrows* show the resulting self-consistent directions of the magnetic moments. *Thin arrows* show the experimental magnetic structure. (b) Projection of the orthorhombic unit cell onto the $xy$ plane. Both experimental and theoretical projections of the magnetic moments are parallel to the $y$-axis. (c) Projection of the monoclinic unit cell onto the $xy$ plane. *Arrows* show schematically the deviations of the magnetic moments from the $yz$ plane

affect the symmetry of the system because the magnetic structure has already lowered the symmetry of the crystal from hexagonal to orthorhombic. As a result, no qualitative changes of the magnetic structure were observed due to the orthorhombic lattice distortion and quantitative changes also appeared to be very small.

A basically different response was obtained to the monoclinic distortions [45]. In agreement with experiment the $b$-side of the basal rectangle (Fig. 5.8) was rotated by $0.4°$ about the $c$-axis. We started the calculations with the magnetic structure I. Already after the first iteration all uranium magnetic moments deviated from the $yz$ plane staying, however, mutually equivalent. The compensating character of the magnetic structure was also preserved.

Again, a symmetry analysis helps to understand this process. The monoclinic distortion decreases the symmetry of the system such that only one half of the symmetry operations of the orthorhombic structure are left over in this case. These are the operations numbered in Table 5.2 as 1, 2, 5, and 6. Operation 5 demands equivalence of atom 1 to atom 3 and atom 2 to atom 4. Simultaneously, the moments of the equivalent atoms must be antiparallel: $m_1 = -m_3$ and $m_2 = -m_4$. Operation 2 is responsible for the equivalence of atoms 1 and 4 and the following relation between the components of the magnetic moments: $m_x^1 = -m_x^4$, $m_y^1 = -m_y^4$, $m_z^1 = m_z^4$. Thus, we see the important difference between the orthorhombic and the monoclinic struc-

**Table 5.2.** Symmetry properties of the orthorhombic UPdSn

$$\varepsilon = \begin{pmatrix} 1 & & \\ & 1 & \\ & & 1 \end{pmatrix}; \quad C_{2z} = \begin{pmatrix} -1 & & \\ & -1 & \\ & & 1 \end{pmatrix}; \quad \sigma_x = \begin{pmatrix} -1 & & \\ & 1 & \\ & & 1 \end{pmatrix}; \quad \sigma_y = \begin{pmatrix} 1 & & \\ & -1 & \\ & & 1 \end{pmatrix}$$

$\tau_1 = \frac{1}{2}(a,b,c); \quad \tau_2 = \frac{1}{2}(a,b,0); \quad \tau_3 = \frac{1}{2}(0,0,c) \; ; R$ time reversal operation

| | Operation | Transposition of U atoms | Restriction on U moments |
|---|---|---|---|
| 1 | $\{\varepsilon\|0\}$ | no | no |
| 2 | $\{C_{2z}\|\tau_1\}$ | $1 \leftrightarrow 4 ; 2 \leftrightarrow 3$ | $\begin{pmatrix} m_x \\ m_y \\ m_z \end{pmatrix}_i = \begin{pmatrix} -m_x \\ -m_y \\ m_z \end{pmatrix}_j ; i \leftrightarrow j$ |
| 3 | $\{\sigma_x\|\tau_2\}$ | $1 \leftrightarrow 3 ; 2 \leftrightarrow 4$ | $\begin{pmatrix} m_x \\ m_y \\ m_z \end{pmatrix}_i = \begin{pmatrix} m_x \\ -m_y \\ -m_z \end{pmatrix}_j ; i \leftrightarrow j$ |
| 4 | $\{\sigma_y\|\tau_3\}$ | $1 \leftrightarrow 4 ; 2 \leftrightarrow 3$ | $\begin{pmatrix} m_x \\ m_y \\ m_z \end{pmatrix}_i = \begin{pmatrix} -m_x \\ m_y \\ -m_z \end{pmatrix}_j ; i \leftrightarrow j$ |
| 5 | $\{\varepsilon\|\tau_2\}R$ | $1 \leftrightarrow 3 ; 2 \leftrightarrow 4$ | $m_i = -m_j ; \quad i \leftrightarrow j$ |
| 6 | $\{C_{2z}\|\tau_3\}R$ | $1 \leftrightarrow 2 ; 3 \leftrightarrow 4$ | $\begin{pmatrix} m_x \\ m_y \\ m_z \end{pmatrix}_i = \begin{pmatrix} m_x \\ m_y \\ -m_z \end{pmatrix}_j ; i \leftrightarrow j$ |
| 7 | $\{\sigma_x\|0\}R$ | no | $m_x = 0 ; \quad$ all $i$ |
| 8 | $\{\sigma_y\|\tau_1\}R$ | $1 \leftrightarrow 4 ; 2 \leftrightarrow 3$ | $\begin{pmatrix} m_x \\ m_y \\ m_z \end{pmatrix}_i = \begin{pmatrix} m_x \\ -m_y \\ m_z \end{pmatrix}_j ; i \leftrightarrow j$ |

tures of UPdSn: in the monoclinic structure there is no symmetry operation demanding the $x$ component of the magnetic moments to be zero. This means that a deviation of the magnetic moments from the $yz$ plane does not change the symmetry of the system and therefore will take place according to our symmetry principle. Thus, the result of the calculation for the monoclinically distorted lattice and the corresponding symmetry analysis are in agreement with the experimental data.

## 5.7 Relativistic Instability of a Compensated Noncollinear Magnetic Structure in Mn$_3$Sn

The magnetic structure in Mn$_3$Sn is very close to compensated triangular. There is, however, a weak ferromagnetic component [46].

In an earlier paper, Sticht et al. [22] studied a number of magnetic configurations allowed by Landau's theory of phase transitions, but SOC was neglected. These calculations showed that, compared to other magnetic states, the triangular configurations have a distinctly lower total energy. Four of the triangular structures are represented in Fig. 5.9. Calculations without SOC showed that all four configurations are equivalent. Another property of all four configurations is their stability during iterations.

The account for SOC changes the situation drastically [7]. First, the degeneracy is lifted, i.e. all four magnetic configurations become inequivalent and, second, for two of them (c and d) the magnetic moments deviate from the initial directions, as depicted in Fig. 5.9. The symmetry analysis shows that structures a and b correspond to symmetry constraint I and are stable in the calculations. Structures c and d correspond to symmetry constraint II
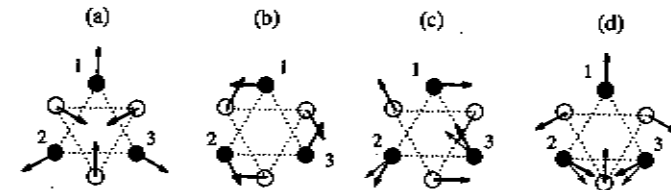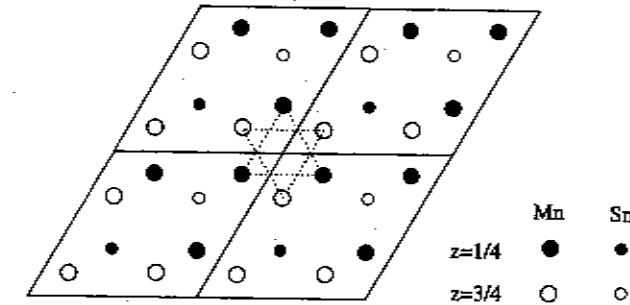


(a)    (b)    (c)    (d)

**Fig. 5.9.** Crystal and magnetic structure of Mn$_3$Sn. Rotations of the magnetic moments leading to weak ferromagnetism in structures (c) and (d) are shown only for atoms in the $z = 0.25$ plane (*thin arrows*). Moments of the atoms in the $z = 0.75$ plane are parallel to the moments of the corresponding atoms of the $z = 0.25$ plane

and are unstable. It is interesting that the weak ferromagnetism in $Mn_3Sn$ is different from the weak ferromagnetism in $Fe_2O_3$ and cannot be attributed to the anisotropic exchange interaction. The symmetry principle of the magnetic instability is, however, universal and can be applied to both cases of weak ferromagnetism.

## 5.8  Nonmagnetic Sublattices in Antiferromagnetic Systems

In this section we show that symmetry principle is useful in the study of the state of the nonmagnetic sublattices in antiferromagnetic systems. Although the atoms of a nonmagnetic sublattice do not develop an independent magnetism, the properties of these atoms are influenced by the interaction with the electron states of the atoms of the antiferromagnetic subsystem.

### 5.8.1  Intersublattice Interaction in $UFe_4Al_8$

For a number of years the magnetic structure of $UFe_4Al_8$ was the matter of much controversy. The suggestions made on the basis of different experimental investigations ranged from simple one-sublattice ferromagnetism up to unusual spin-glass state [47]. Recent investigation of a single crystal of $UFe_4Al_8$ with the use of unpolarized and polarized neutron diffraction revealed an ordered magnetic structure with a number of unique features [48] (Fig. 5.10). Two magnetic sublattices were detected. The magnetic moments of the U sublattice form a collinear ferromagnetic structure. A strong noncollinearity is, however, observed between the U and Fe magnetic moments, which are almost orthogonal to one another. The magnetic structure of the Fe sublattice is close to a collinear antiferromagnetic (so called G-type antiferromagnetic structure). Additionally, there is a canting of the Fe moments, which leads to the second type of noncollinearity in $UFe_4Al_8$. The noncollinearity within the Fe sublattice results in a weak ferromagnetic moment parallel to the U moments.

In [26] we have shown that the complex noncollinear magnetic structure of $UFe_4Al_8$ is a necessary consequence of the properties of a much simpler magnetic state with collinear antiferromagnetism of the Fe sublattice and nonmagnetic U sublattice (Fig. 5.10). To stress the importance of this state for understanding of the magnetism of $UFe_4Al_8$ we refered to it as the basic state (BS).

The BS possesses a number of regular features: the Fe atoms have equal magnetic moments, these magnetic moments are collinear, the magnetic moment of the U atoms has the value of zero. We emphasize that the property that the U moment is equal to zero must be considered as a regular feature of the system, which can be stable only in the case that there exists a symmetry
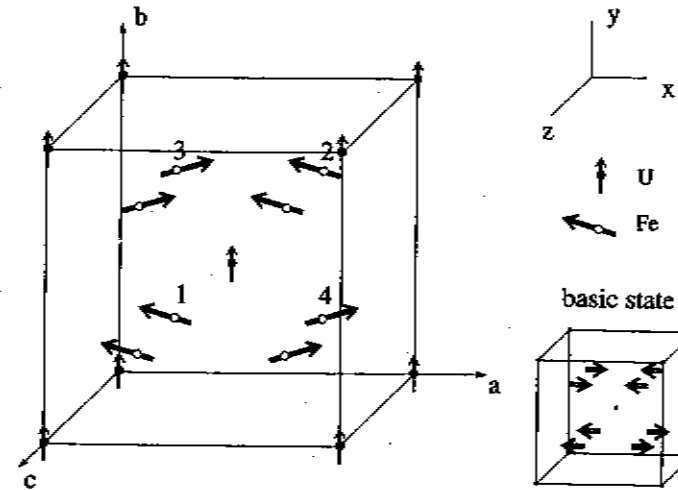
Fig. 5.10. Experimental magnetic structure and basic magnetic state of $UFe_4Al_8$

operation that is responsible for the stability of this feature in the sense of our symmetry criterion.

The DFT calculation started with the BS [26] shows immediately that two of these three regular features are not preserved by the system: An induced moment appears at the U site. It is orthogonal to the initial directions of the Fe moments. Simultaneously, the Fe moments deviate from their collinear directions and form a canted noncollinear configuration. Thus, the BS is transformed into the complex magnetic state observed experimentally. Symmetry analysis helps to understand the origin of this transformation.

In Table 5.3 we collect the generators of the symmetry group of the BS of $UFe_4Al_8$. One of the interesting questions to answer is about the physical mechanism of breaking, by the planar magnetic state of the BS, the symmetry between two opposite directions of the b-axis. Indeed, the ferromagnetism of the U sublattice distinguishes one of the two directions. Two opposite directions of the U magnetic moments can be equivalent only in the case when there is a symmetry operation of the system that reverses the direction of the magnetic moment. In the present case it must be an operation that reverses $m_y$. Analysis of Table 5.3 shows that this condition is not fulfilled. All symmetry transformations leave $m_y$ invariant. As a direct consequence of this property the appearance of a magnetic moment parallel to the y-axis at the U sites does not disturb any of the symmetry operations. Therefore we deal here with symmetry constraint II where the value of the U magnetic moment plays the role of the variable parameter. The symmetry predetermined instability of

**Table 5.3.** Generators of the symmetry group of the basic state of $UFe_4Al_8$ $C_{2x}$ and $C_{2y}$ are 180° rotations about the $x$- and $y$-axis, respectively; $I$ inversion; $R$ time reversal. In the last column, for the U sublattice $i = j$; for the Fe sublattice $i$ and $j$ according to the column "Transposition of the Fe atoms"

| Operation | Transposition of Fe atoms | Restriction on magnetic moments of U and Fe atoms |
|---|---|---|
| $C_{2y}$ | $1 \leftrightarrow 3$ ; $2 \leftrightarrow 4$ | $\begin{pmatrix} m_x \\ m_y \\ m_z \end{pmatrix}_i = \begin{pmatrix} -m_x \\ m_y \\ -m_z \end{pmatrix}_j$ |
| $I$ | no | no |
| $C_{2x}R$ | $1 \leftrightarrow 4$ ; $2 \leftrightarrow 3$ | $\begin{pmatrix} m_x \\ m_y \\ m_z \end{pmatrix}_i = \begin{pmatrix} -m_x \\ m_y \\ m_z \end{pmatrix}_j$ |

the nonmagnetic state of the U atoms can be illustrated by the properties of the total energy as a function of $m_y$ (Fig. 5.11). The most important feature of the $E(m)$ curve is its asymmetry, which leads to an accidental position of the minimum at a nonzero value of $m_y$.

The orthogonality of the inducing and induced moments is also closely connected with the symmetry properties of the system since the appearance of a nonzero $m_x$ or $m_z$ component of the U moment would disturb at least one of the symmetry operations of the BS.
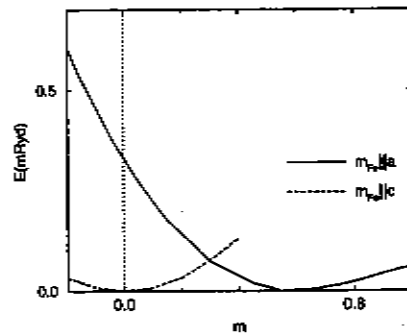


**Fig. 5.11.** Total energy as a function of the U spin moment for the Fe moments collinear to the $a$- (basic state) and $c$-axes. For the Fe moments parallel to the $c$-axis no induced U moment appears

The same symmetry analysis shows that the collinear directions of the Fe moments are also not distinguished by symmetry and cannot be stable. Both $m_y$ and $m_z$ components of the moments must appear. To preserve the symmetry of the BS the $m_z$ components of different atomic moments have different signs and compensate one another. On the other hand, the $m_y$ components of all atomic moments are equal and, in agreement with experiment, result in a weak ferromagnetic moment along the $b$-axis.

Summarizing, if the appearance of the induced moments on nonmagnetic atoms in an antiferromagnetic system does not destroy any of the symmetry operations of the system, these moments must appear. The directions of the induced moments do not necessary coincide with the directions of the induced moments and are determined by the condition that the symmetry of the magnetic system must be preserved.

We emphasize that the symmetry analysis and DFT calculations reported in this section were performed taking account of the SOC. With the SOC neglected, none of the effects discussed here appear and the BS is stable.

### 5.8.2   Magnetic Structure of $UX_3$ Compounds

In [49] we have shown that the relation between the inducing and induced moments that follows from the symmetry analysis discussed in the previous sections can be helpful in the determination of the magnetic structure of the inducing subsystem. In $UX_3$ neutron diffraction did not provide complete information about the magnetic structure of the U sublattice. Since, according to our symmetry principles, different directions of the U magnetic moments result in different properties of the induced moments of the X atoms, the study of the induced moments provides information about the magnetic structure of the U sublattice. Measuring the hyperfine field on the positions of X atoms with, for example, the perturbed-angular-correlation technique allows us to draw the conclusions about the induced moments. Figure 5.12 illustrates the properties of induced moments of the X atoms for different orientations of the U moments. The reader is referred to [49] for full details of the study of the magnetic structure of $UX_3$ compounds.

## 5.9   Helical Structures in Systems with Relativistic Interactions

A wide variety of systems has been reported to possess a helical magnetic order with the periodicity incommensurate with the periodicity of the crystal lattice (see, e.g. [50,51]). However, almost all DFT calculations of helical magnetic configurations have been carried out for one system: $\gamma$-Fe [52,53]. (For an exception, see the recent study on the rare-earth metals [54].) The reasons for the concentration on $\gamma$-Fe are connected with a negligible role of the SOC in the formation of the magnetic structure in this system. Here, we
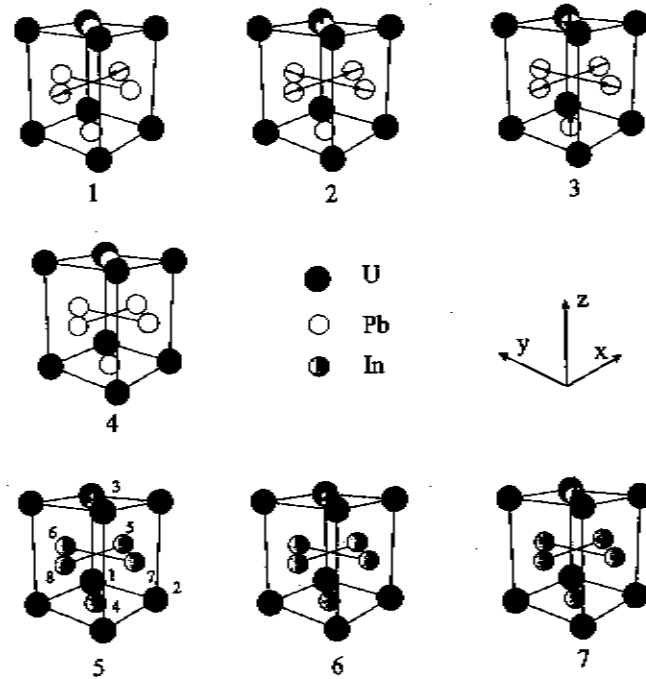
Fig. 5.12. Models for the magnetic structure of $UX_3$ compounds. The induced magnetic moments on sites that follow from the symmetry analysis are shown. See [49] for all details

consider two examples of the systems where helical magnetic structures were reported to be observed and the role of the SOC cannot be neglected.

### 5.9.1   Magnetic Structure of UPtGe

In accordance with the experimental situation we consider [27] plane helical magnetic structures of the form

$$e_\nu^q = (\cos(qa_\nu + \phi_o), 0, \sin(qa_\nu + \phi_o)),    (5.10)$$

where the $a_\nu$ are the positions of the U atoms and $q$ is the helix vector. Although not periodic with the underlying lattice periodicity, the helical structure is very regular. This regularity can be described by the generalized translations [11] that combine lattice translations $R_n$ with spin rotations by

$qR_n$ about the $y$-axis. The scalar-relativistic Hamiltonian of the helix commutes with the generalized translations. This property allows us to reduce the consideration of the incommensurate helical magnetic structure to a problem in one chemical unit cell of the crystal and thereby drastically simplifies the calculations.

The role of the symmetry with respect to the generalized translations is not, however, restricted to the technical convenience. This symmetry is crucial for the stability of the regularities characteristic of a helix. The spin-orbit coupling term of the Hamiltonian does not commute with the generalized translations. Therefore, the relativistic Hamiltonian cannot be invariant with respect to the generalized translations. This leads to the instability of the incommensurate helical structures for the systems where the SOC plays an important role in the formation of the magnetic structure. The physical reason for the distractive role of the SOC can be easily understood. Indeed, regularity inherent in the helices assumes that only the relative directions of the magnetic moments are important, but not their directions with respect to the crystal lattice. The SOC connects the space and spin degrees of freedom and makes inequivalent different orientations of the moments with respect to the lattice. The destructive role of the SOC provides an explanation for the fact that the main body of the DFT studies of helical structures is restricted to the case of the helical structure in $\gamma$-Fe where the SOC can be neglected.

A much more complex situation exists in the case of rare-earth metals (REM) [51]. Here, the exchange interaction favors the formation of a helical structure. However, the influence of the SOC is stronger than in $\gamma$-Fe and cannot be neglected.

A further increase of the role of the SOC can be expected in the case of actinide systems. The considerable spatial extent of the 5f electron states enhances the influence of the SOC on the directions of the atomic moments. This property is confirmed by the observation of a large magnetic anisotropy (see, e.g. [55]) in almost all actinide compounds. Taking into account the influence of the SOC on helical structures, the formation of a helix in U compounds can be considered as highly improbable [11,56]. This conclusion seems to be in good agreement with the experimental observations. There is, however, one exception: UPtGe (Fig. 5.13) was reported to possess a helical ground-state structure [57,58]. An understanding of the nature of the unique magnetism of UPtGe is essential for the physics of incommensurate magnetic structures. On the other hand, the unique magnetic structure makes UPtGe an important test case for the verification of the capability of DFT to explain the complex magnetism in 5f systems. Below, we discuss the explanation of the properties of UPtGe suggested by Sandratskii and Lander [27].

Two different types of helices are known. The first type is formed, for example, in fcc-Fe and REM and results from the properties of the exchange interactions. Neglecting the SOC and considering the total energy of the helix as a function of $q$, $E_{ex}(q)$, one obtains the minimum at an incommensurate
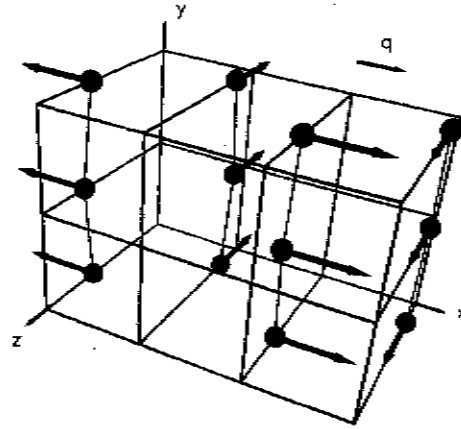
**Fig. 5.13.** The U positions in UPtGe. The magnetic structure shown corresponds to $q = (0.5, 0, 0)$ and is a helix with the moments in the $xz$ plane with the propagation along $x$. Experimental value of $q$ is $(0.55–0.57, 0, 0)$ [57,58]
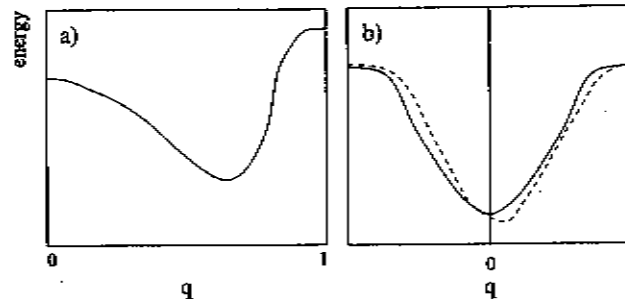


**Fig. 5.14.** Schematic picture of the total energy as a function of $q$ for (a) exchange and (b) relativistic helices

$q$ value (Fig. 5.14a). As stated above, such a helix can be formed only in the case when the MA is much weaker than the interatomic exchange interactions determining the form of the $E_{ex}(q)$ function.

In apparent contradiction to the arguments above, the second type of helices is formed because of the influence of SOC, e.g. the helix in MnSi [59,60]. The exchange interaction in MnSi favors a collinear ferromagnetic ordering. This means that the minimum of the total energy as a function of $q$, calculated nonrelativistically, is at $q = 0$ (Fig. 5.14b). To explain the formation of the helix in MnSi a model Hamiltonian was used (see, e.g. [59]),

which, in addition to the exchange interaction contains the Dzyaloshinski-Moriya interaction (DMI) $D(S_1 \times S_2)$. Although the DMI is a consequence of the SOC, the simultaneous rotation of all atomic moments about the direction of the $D$ vector does not change the energy of the system. This property of the DMI allows the symmetry of the system with respect to the generalized translations to be maintained, which is a necessary condition for the stability of helical structures. On the other hand, the DMI term disturbs the symmetry of the $E(q)$ curve with respect to the reversal of $q$ and leads to the shift of the minimum of the total energy to an incommensurate $q$.

The DMI is not, however, the only interaction resulting from the SOC. Another term, the magnetic anisotropy [36,59] (MA), destroys the symmetry of the problem with respect to the generalized translations. Therefore, to allow the formation of the helical structure of the MnSi type the SOC must be present, but the magnetic anisotropy must be smaller than the DMI. Since, under certain conditions [36], the DMI is proportional to the SOC, and the MA to the square of the SOC, these requirements can be fulfilled in the case of weak SOC, e.g. in MnSi. The long period (180 Å) of the helix in MnSi is a reflection of the weakness of the relativistic effects.

Since for both types of helices the smallness of the magnetic anisotropy is important, we studied this quantity and compared its value with the value of the interatomic exchange interactions. To estimate the MA we compare the total-energy differences between the magnetic structures with the same relative orientation of the atomic moments but different orientation with respect to the crystal lattice (Table 5.4). The interatomic exchange interaction is estimated by comparison of the total energies of the ferromagnetic and antiferromagnetic configurations with atomic moments collinear to an axis.

Calculations show that the MA in the $xz$ plane is very small. Since the SOC is strong and there is no symmetry reason for the smallness of the inplane anisotropy this property results from an accidental compensation of the contributions of different electron states. An estimation of the exchange interaction shows that it is much stronger than the inplane magnetic anisotropy [27].

The weakness of the inplane magnetic anisotropy is a necessary condition for the formation of the helical structure. It does not, however, provide the physical mechanism leading to the formation of the helix. In Fig. 5.15 we show the $q$ dependence of the total energy that was calculated neglecting the SOC. A clear trend to the formation of the helix with an incommensurate $q$ value close to 0.5 is obtained.

On the basis of the Fourier transformation of the $E(q)$ curve the following qualitative picture of the magnetism of UPtGe was suggested. The U positions in UPtGe form a structure rather close to a simple hexagonal (Fig. 5.16). The effective exchange interaction between the magnetic moments of atoms 0 and 2 is strong and antiferromagnetic. The exchange interaction of the magnetic moments of atoms 1 and 3 with the moments of atoms 0 and 2 is

**Table 5.4.** Important energy differences in mRyd/U atom. The energy of magnetic anisotropy is estimated as the total-energy difference between the magnetic structures with the same relative orientation of the atomic moments but different orientation with respect to the crystal lattice. The interatomic exchange interaction is estimated as the difference of the total energies of the ferromagnetic and antiferromagnetic configurations with atomic moments collinear to the same axis

| Magnetic anisotropy | |
|---|---|
| $E_{FM}(010)-E_{FM}(100)$ | 1.5 |
| $E_{FM}(010)-E_{FM}(001)$ | 1.4 |
| $E_{FM}(001)-E_{FM}(100)$ | 0.1 |
| $E_{AFM}(010)-E_{AFM}(100)$ | 1.3 |
| $E_{AFM}(010)-E_{AFM}(001)$ | 1.2 |
| $E_{AFM}(001)-E_{AFM}(100)$ | 0.1 |
| Exchange interaction | |
| $E_{AFM}(100)-E_{FM}(100)$ | −0.1 |
| $E_{AFM}(010)-E_{FM}(010)$ | −0.3 |
| $E_{AFM}(001)-E_{FM}(001)$ | −0.2 |
| $E_{q=(0.5,0,0)}-E_{FM}(100)$ | −0.8 |
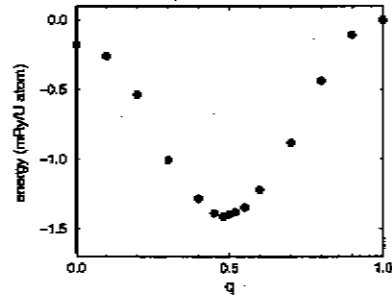


**Fig. 5.15.** Energy as a function of $q = (q, 0, 0)$

much weaker. Evidently the antiparallel directions of the moments 0 and 2 lead to the frustration of the direction of the moments 1 and 3. The frustrated magnetic interactions are the reason for the minimum of the total energy at an incommensurate $q$ value (Fig. 5.15). This result suggests that the helical magnetic structure in UPtGe should be considered as an exchange helix.

One further remarkable experimental feature of UPtGe is, however, the observation of the domains of only one chirality [58]. This property is characteristic of the relativistic helices of the MnSi type [60]. In [27] we have shown
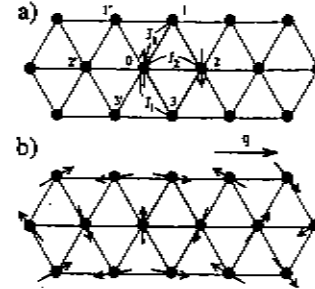


**Fig. 5.16.** Frustrated magnetic interactions. (a) $|J_2| \ll |J_1|$. (b) Helical magnetic structure as a consequence of the frustration
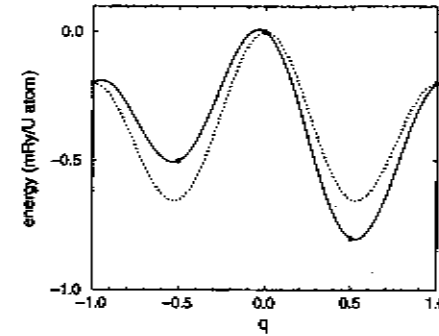


**Fig. 5.17.** $E(q)$ without DMI (*dotted line*) and with DMI (*solid line*). See [27] for all details

that the inequivalence of the domains of opposite chirality in UPtGe is a result of the SOC which leads to a substantial DMI in the system. Figure 5.17 shows the total energy as a function of $q$ evaluated with and without the DMI interaction. Summarizing, an accidentally small inplane magnetic anisotropy provides a necessary condition for the formation of the incommensurate helix. The formation and properties of the helix are determined by the frustrated exchange interactions and relativistic DMI. The magnetic structure of UPtGe cannot be classified either as a pure exchange or pure relativistic helix, but possesses the features of both.

### 5.9.2   Helices in REM

A rich variety of complex magnetic configurations was experimentally found in the heavy REM [51,61]. An important contribution to the understanding of

the magnetic properties of heavy REM is made by Jensen and collaborators (see the book [51] and references therein and later publications, e.g. [62]) who used a model spin-Hamiltonian to describe peculiar magnetism in these systems. (See also [63] for an earlier phenomenological theory of the magnetic ordering in REM.)

In contrast to the model-Hamiltonian approach, the contribution of the DFT to the study of the complex magnetism in heavy REM is very modest. Most of the DFT calculations for REM were performed for the collinear ferromagnetic structure of Gd. To the best of the author's knowledge, only two direct first-principles DFT calculations of complex magnetic configurations in heavy REM were reported. Nordström and Mavromaras [54] used the scalar-relativistic approximation to study the $q$ dependence of the total energy of planar spiral structures. Here, $q$ is the propagation vector of the spiral. The $E(q)$ curves were compared with the Fourier components of the interatomic exchange parameter $J(q)$ determined experimentally. Perlov et al. [64] employed a scalar-relativistic approximation to calculate $J(q)$ by examining the conical spiral configurations. No studies of the influence of the SOC on the magnetic configurations of heavy REM have been performed within the framework of the DFT. The success of the DFT in the investigation of the magnetic properties of solids and recent developments in the computational techniques and facilities make the complex magnetism of the heavy REM one of the important topics for nearest-future studies. Combination of the model-Hamiltonian and first-principles DFT approaches should provide a new level of the theoretical description of REM magnetism.

It is not a purpose of this chapter to report a detailed DFT study of the magnetism of concrete REM. Rather we aim to provide one example of the usefulness of the symmetry analysis and relativistic DFT calculations in the studies of the REM.

In the calculations, the 4f states were treated as pseudocore [65] states and did not hybridize with the valence electron states. A scalar-relativistic approximation was used in the description of the core states. The SOC was considered for the valence electrons only. The neglect of the SOC in the 4f states is a severe approximation in the physical model describing the effects of the magnetic anisotropy in REM. For example, the SOC in the 4f states plays an important role in the description of the magnetic properties of the 4f metals in terms of the model crystal-field Hamiltonian [51]. Neglecting the SOC in the 4f states we can expect that the strength of the magnetic anisotropy will be substantially underestimated. To simulate a stronger magnetic anisotropy within the given calculational scheme in some cases we performed calculations with the SOC enhanced by a factor of 20.

Several REM were reported to possess a helical magnetic structure. Thus, a planar helix is observed in certain temperature intervals in Tb, Dy, Ho, and Er. A ferromagnetic helix (cone structure) is observed in Ho and Er.

**Table 5.5.** Generators of the symmetry groups for three magnetic states in hcp metals. Number of atoms in the magnetic unit cell $n_{at}$ characterizes the periodicity of the magnetic structure along the $c$-axis. $C_{2b}$ is the $180°$ rotation about the $b$-axis; $\sigma_a$ and $\sigma_c$ are the reflections in the plane orthogonal to the axes $a$ and $c$, respectively; $R$ time reversal. Vectors in the column "Operation" give the nonprimitive translations entering the symmetry operations. Vectors are given in units of $c$. Atoms not presented in the column "Transposition" are invariant with respect to the given symmetry operation. In the last column,

$$\text{type } C_{2a}: \begin{pmatrix} m_a \\ m_b \\ m_c \end{pmatrix}_j = \begin{pmatrix} m_a \\ -m_b \\ -m_c \end{pmatrix}_i ; \text{type } C_{2b}: \begin{pmatrix} m_a \\ m_b \\ m_c \end{pmatrix}_j = \begin{pmatrix} -m_a \\ m_b \\ -m_c \end{pmatrix}_i ;$$

$$\text{type } C_{2c}: \begin{pmatrix} m_a \\ m_b \\ m_c \end{pmatrix}_j = \begin{pmatrix} -m_a \\ -m_b \\ m_c \end{pmatrix}_i ; \text{type } R: m_j = -m_i. \text{ Here } i \text{ and } j \text{ according}$$

to the column "Transposition". Atom $i$ is transformed to atom $j$ under the action of the symmetry operation. For atoms invariant under the action of the symmetry operation, $j = i$

| Magnetic structure | $n_{at}$ | Operation | Transposition | Restriction on magnetic moments |
|---|---|---|---|---|
| helix, $ab$-plane | 8 | $C_{2b}$ | $2 \leftrightarrow 8; 3 \leftrightarrow 7; 4 \leftrightarrow 6;$ | type $C_{2b}$ |
| (Fig. 5.18a) | | $R(0,0,2)$ | $1 \leftrightarrow 5; 2 \leftrightarrow 6; 3 \leftrightarrow 7; 4 \leftrightarrow 8;$ | type $R$ |
| cycloid, $bc$-plane | 8 | $C_{2b}$ | $2 \leftrightarrow 8; 3 \leftrightarrow 7; 4 \leftrightarrow 6;$ | type $C_{2b}$ |
| (Fig. 5.18b) | | $\sigma_a(0,0,2)$ | $1 \leftrightarrow 5; 2 \leftrightarrow 6; 3 \leftrightarrow 7; 4 \leftrightarrow 8;$ | type $C_{2a}$ |
| | | $R(0,0,2)$ | $1 \leftrightarrow 5; 2 \leftrightarrow 6; 3 \leftrightarrow 7; 4 \leftrightarrow 8;$ | type $R$ |
| cycloid, $ac$-plane | 8 | $\sigma_c(0,0,2)$ | $1 \leftrightarrow 5; 2 \leftrightarrow 4; 6 \leftrightarrow 8;$ | type $C_{2c}$ |
| | | $R(0,0,2)$ | $1 \leftrightarrow 5; 2 \leftrightarrow 6; 3 \leftrightarrow 7; 4 \leftrightarrow 8;$ | type $R$ |

Here, using the example of Er, we will consider the influence of the SOC on the helical magnetic structures in REM. A more extensive discussion can be found [66].

In the case of Er, the structures with $q = \frac{1}{4}$ are of interest [51]. First, we consider the influence of the SOC on a planar helix with $q = \frac{1}{4}$ (Fig. 5.18a). The generators of the symmetry group are given in Table 5.5. There are three groups of equivalent atoms: $\{1,5\}$, $\{3,7\}$, $\{2,4,6,8\}$. The moments of atoms 1 and 5 must keep their initial directions parallel to the $b$-axis. Atomic moments 3 and 7 deviate within the $ac$ plane, no $b$ component can appear. Moments 2, 4, 6, 8 move both within the $ab$ plane and out of the $ab$ plane. No ferromagnetic component can appear.

Numerical calculations started with this helical structure gave an interesting result that differs drastically with the results obtained in the calculations for Ho. For the SOC scaled by a factor of 20 the moments deviate
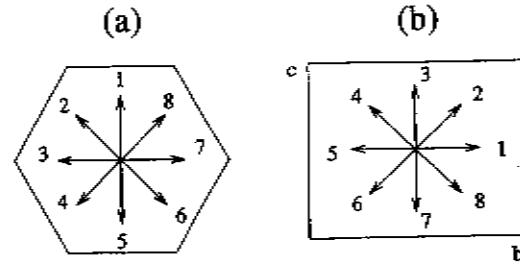
**(a)**                    **(b)**



Fig. 5.18. The 8-layer magnetic configurations in hcp Er. (a) The initial planar helical structure. All moments are parallel to the $ab$ plane. (b) The calculated planar magnetic structure. All moments are parallel to the $bc$ plane

strongly from the $ab$ plane and result in the magnetic configuration shown in Fig. 5.18b. Thus, the initial planar magnetic configuration with moments parallel to the horizontal $ab$ plane is replaced by a planar magnetic structure parallel to the vertical $bc$ plane. This transformation of the magnetic configuration is not forbidden by symmetry since all the symmetry elements of the initial structure are preserved. The final magnetic state is more symmetrical than the initial one since the symmetry group contains one additional generator (Table 5.5). This example illustrates the property that the symmetry of the state of the system can increase in the calculations. The planar vertical structure obtained in the calculations is in good agreement with a vertical planar cycloidal structure found experimentally in Er. Two structures are, however, not identical: The calculations resulted in a structure parallel to the $bc$ plane. The experimental structure is parallel to the $ac$ plane. A wobbling of the vertical structure found experimentally is also not reproduced in this calculation. The reason for this disagreement is, again, connected with the symmetry of the initial state. Indeed, the structure shown in Fig. 5.18a cannot transform within the DFT calculations into the planar structure parallel to the $ac$ plane since this transformation leads to a loss of symmetry operations.

To understand the nature of the wobbling of the experimental vertical structure we performed the symmetry analysis for a magnetic configuration shown in Fig. 5.18b but, in this case, parallel to the $ac$ plane. The symmetry of this structure preserves (i) the directions of the atomic moments 3 and 7, (ii) the zero $c$ component of the moments 1 and 5, and (iii) the compensated character of the structure as a whole. Moments 2–4 and 6–8 deviate from the $ac$ plane leading to the wobbling observed experimentally. Note that a model spin-Hamiltonian that contains only the terms of the second-order with respect to atomic spins: the Heisenberg exchange interaction and the single-site magnetic anisotropy, fails to describe the wobbling. The fourth-order 'trigonal' interactions must be added [62]. In the magnetic and relativistic

DFT calculations these and higher-order interactions are automatically taken into account.

Since the magnetic anisotropy is very sensitive to the details of the theoretical model, future systematic DFT studies of the REM magnetism should consider such effects as polar magnetic interaction of atomic moments and lattice distortion caused by magnetoelastic interactions [63]. The account for the SOC in the 4f states is of great importance. Another important direction for the improvement of the calculational scheme is a better account for the correlation effects in the 4f states. Here, self-interaction corrections, [67] orbital polarization corrections [68] or an LDA+U [69] scheme should be considered as possible approaches. Combination of these improvements should make possible a first-principles quantitative description of the delicate balance of different interactions traditionally described in terms of a model crystal-field Hamiltonian [51]. Detailed DFT study of the magnetism of heavy REM with account for the SOC and noncollinearity of the magnetic structure is an exciting topic for the nearest-future researches. The symmetry analysis reported here preserves its validity also for more elaborate physical models. We hope that the present symmetry analysis and results of numerical calculations will stimulate further studies of the complex magnetism in REM systems.

## 5.10   Intraatomic Magnetic Noncollinearity

We will briefly comment on two important aspects of the intraatomic magnetic noncollinearity. The first aspect is the spatial variation of the direction of magnetization within the volume of an atom [4,6,21,70,71] (Fig. 5.19). As already mentioned in Sect. 5.2, in any relativistic magnetic system the intraatomic spin density is always noncollinear. In terms of symmetry arguments, this is an inevitable consequence of the property that the spin projection on any selected axis cannot be a good quantum number characterizing electron states. Also, the orbital intraatomic magnetization is noncollinear [72], though the concrete form of the orbital magnetization depends strongly on the gauge chosen. In nonrelativistic systems, a collinear intraatomic spin density is possible if the magnetic moments of different atoms are collinear.

Another type of intraatomic magnetic noncollinearity is the noncollinearity of the spin and orbital magnetic moments of the same atom [5,56,73]. The collinearity of both atomic moments must be considered as a regularity in the system that, according to our symmetry principle, is possible only in the case that there is a symmetry operation that is responsible for this regularity. In all cases where *interatomic* magnetic noncollinearity is predetermined by symmetry (symmetry constraint II) the atomic spin and orbital moments are also noncollinear. (See, e.g. [5,56,73] for calculations of concrete systems.)
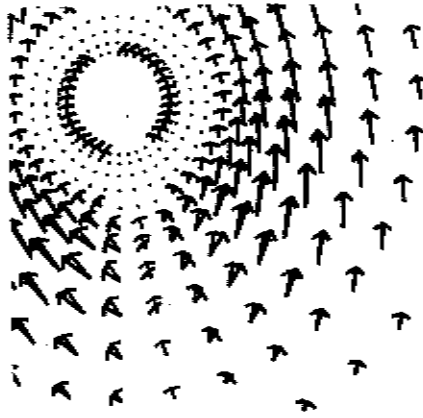
Fig. 5.19. Intraatomic spin magnetization in a U atom in $U_3Bi_4$ obtained in self-consistent (*black arrows*) and nonself-consistent (*grey arrows*) calculations. See [21] for all details

## 5.11  Relativistic Spectroscopy of Noncollinear Magnetic States

The SOC plays a crucial role in the magneto-optical Kerr effect of magnetic systems. Here, we briefly discuss the first DFT study of the magneto-optical Kerr effect (MOKE) of a noncollinear system [74]. (See also [77] for a recent relativistic calculation of photoemission and X-ray absorption spectra of systems with noncollinear magnetic configuration.)

The calculation was performed for the $U_3P_4$ compound (see Sect. 5.5.1) for different values of the cone angle (Fig. 5.5). Both optical and magneto-optical properties of a system can be deduced from the optical conductivity tensor $\sigma(\omega)$. The expression for $\sigma(\omega)$ contains interband and intraband contributions. The interband part can be represented in the following form

$$\sigma_{\alpha,\beta}^{inter}(\omega) = \frac{ie^2}{m^2 V} \sum_{k \in 1.BZ} \sum_{\substack{n,m \\ n \neq m}} \frac{f(E_{n,k}) - f(E_{m,k})}{E_{m,k} - E_{n,k}}$$

$$\times \frac{<n,k|p_\beta|m,k><m,k|p_\alpha|n,k>}{\omega - \frac{E_{m,k}-E_{n,k}}{\hbar} + i\delta},\qquad (5.11)$$

where $\omega$ is the frequency of the incident photons, $E_{n,k}$ is the energy of the electron eigenstate $|n,k>$ labeled with the band index $n$ and vector $k$ in the first Brillouin zone. Furthermore, $p_\alpha$ is the $\alpha$-component of the electron momentum operator, $f(E)$ is the Fermi-Dirac function, and $\delta$ is a phenomenological parameter describing finite-lifetime broadening. The comparison with

experiment was carried out with the normal-incidence reflectivity and the polar Kerr rotation [74]. Assuming the $z$-axis to be normal to the surface of the crystal the reflectivity takes the following form

$$R = \frac{(n-1)^2 + k^2}{(n+1)^2 + k^2}, \quad n + ik = \sqrt{1 + \frac{4\pi i}{\omega}\sigma_{x,x}}.$$

The simple expression for the polar Kerr angle,

$$\Phi_K = \Re\left\{ \frac{-\sigma_{x,y}}{\sigma_{z,x}\cdot\sqrt{1 + \frac{4\pi i}{\omega}\cdot\sigma_{z,x}}} \right\}$$

is applicable only in the case when the $z$-axis is a symmetry axis of at least third order (see, e.g. [75]). This is so for $U_3P_4$ where the magnetization is parallel to the crystallographic [111] axis, which is a three-fold symmetry axis. Although the presence of magnetic ordering can substantially decrease the symmetry, for the noncollinear ground-state magnetic structure of $U_3P_4$ the symmetry with respect to the [111] axis stays intact. Thus, by directing the $z$-axis along the crystallographic [111] axis we obtain the geometry necessary for the calculation of the polar magneto-optical Kerr rotation. Note that the expression (5.11) for the optical conductivity tensor is quite general and applicable to both collinear and noncollinear magnetic configurations. The difference between both cases is contained implicitly in the electron eigenenergies and eigenfunctions entering this formula.

To study the sensitivity of the optical characteristics to the canting angle we performed the calculation for different cone angles (Fig. 5.20). The dependence of the reflectivity on the canting angle is seen to be surprisingly weak, whereas the photon-energy dependence of the Kerr rotation practically scales with the macroscopic magnetization given by the projection of the magnetic moments onto the [111] axis. To understand the essential difference in the angular dependence of the reflectivity and the Kerr angle note that the first characteristic is determined by the diagonal component of the conductivity tensor (5.11) in contrast to the second characteristic, which depends crucially on the off-diagonal component of the tensor. Although the same electron transitions contribute to both components the weight of the contribution is different [75]: the absorption part of the diagonal component can be represented as a sum of the corresponding components for the right- and left-circularly polarized light, opposite to the absorption part of the off-diagonal component that can be seen as a difference of the corresponding characteristics for the right- and left-circular polarized light. As a direct consequence of this property, the off-diagonal component of the conductivity tensor must be zero for a canting angle of 90° because in this case all atomic moments are parallel to the $xy$ plane and the right- and left-circularly polarized waves become equivalent. Simultaneously, the Kerr rotation becomes zero. Thus, the monotonic decrease of the Kerr rotation with increasing canting angle
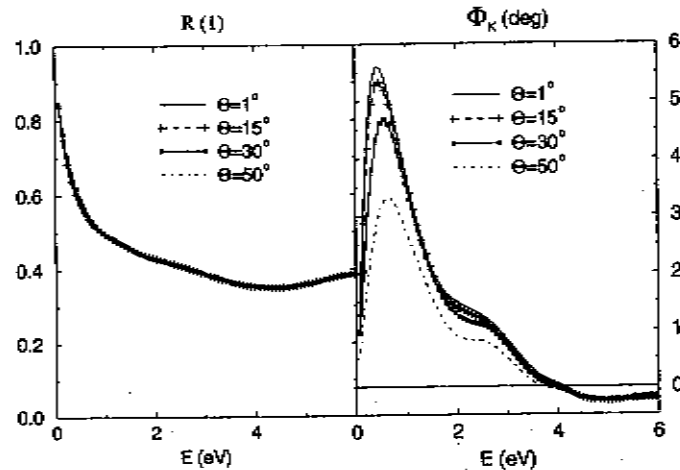
**Fig. 5.20.** Calculated [74] reflectivity (*left*) and polar Kerr rotation spectra (*right*) of $U_3P_4$ for different deviations $\theta$ of the uranium magnetic moments from the crystallographic [111] direction

that is obtained in our calculations can be treated as a natural consequence of the symmetry properties of the magneto-optical effect.

Still, the very high stability of the reflectivity as a function of canting and the simple scaling of the Kerr-rotation peak with respect to the $z$ projection of the magnetic moment are nontrivial. The very weak dependence of the reflectivity on the magnetic structure for the whole range studied can be interpreted as follows. The electron states enter the optical conductivity through the eigenenergies and the matrix elements involving the eigenfunctions, both of which can thus depend only weakly on the change of the directions of the atomic moments. This means, first, the U 5f states – as seen from the *local* atomic coordinate system having the quantization axis parallel to the atomic moment – are almost unchanged for any magnetic configuration. Second, the hybridization of the U 5f states with the nonmagnetic valence states, e.g. P 3p states, does not change substantially with rotation of the U 5f states. These properties result in the weak dependence of the energy values and near invariance of the transition probabilities.

Thus we deal with the case of a well-defined magnetic U moment that is formed by the itinerant 5f electrons: the moments can rotate without substantially changing the 5f electron states as seen from the local atomic reference system. This phenomenon is known from studies of the 3d elements and their compounds [76]. This result is crucial for the understanding of

the properties of the compound at finite temperatures, in particular for the Curie-Weiss behavior of the magnetic susceptibility [76].

## 5.12  Conclusion

Summarizing, we have shown that the spin-orbit coupling plays an important role in the formation of the magnetic structure and properties of noncollinear magnetic systems. The modern density functional theory allows the study of these effects within a parameter-free calculational scheme. We have shown that the analysis of the symmetry aspects of the problem is very helpful in the predicting and understanding the results of the DFT calculation. On the basis of the notion of the symmetry constraint we formulated a symmetry principle of the stability of regular features of the magnetic configuration and demonstrated the efficiency of this principle by application to very different magnetic systems. It is to be expected that noncollinear magnetic states will play an increasing role in the future of solid-state physics. Note, that the modern engineered nanomaterials possess, as a rule, peculiar symmetry properties. This gives the principles and methods discussed here an enormous application potential in the new fields of magnetism.

## References

1. R. Lorenz, J. Hafner, S.S. Jaswal, and D.J. Sellmyer: Phys. Rev. Lett. **74**, 3688 (1995)
2. V.P. Antropov, M.I. Katsnelson, M. van Schilfgaarde, and B.N. Harmon: Phys. Rev. Lett. **75**, 729 (1995)
3. L.M. Sandratskii and J. Kübler: Phys. Rev. Lett. **75**, 946 (1995)
4. L. Nordström and D.J. Singh: Phys. Rev. Let. **76**, 4420 (1996)
5. I. Solovyev, N. Hamada, and K. Terakura: Phys. Rev. Lett. **76**, 4825 (1996)
6. T. Oda, A. Pasquarello, and R. Car: Phys. Rev. Let. **80**, 3622 (1998)
7. L.M. Sandratskii and J. Kübler: Phys. Rev. Lett. **76**, 4963 (1996)
8. M. Uhl and J. Kübler: Phys. Rev. Lett. **77**, 337 (1996)
9. Y. Wang, G.M. Stocks, D.M.C. Nicholson, and W.A. Shelton: J. Appl. Phys. **81**, 3873 (1997)
10. O.N. Mryasov, R.F. Sabiryanov, A.J. Freeman, and S.S. Jaswal: Phys. Rev. **56**, 7255 (1997)
11. L.M. Sandratskii: Adv. Phys. **47**, 91 (1998)
12. Q. Niu, X. Wang, L. Kleinman, W.-M. Liu, D.M.C. Nicholson, and G.M. Stocks: Phys. Rev. Lett. **83**, 207 (1999)
13. M. van Schilfgaarde, I.A. Abrikosov, and B. Johansson: Nature **400**, 46 (1999)

14. A. Taga, L. Nordstrm, P. James, B. Johansson, and O. Eriksson: Nature 406, 280 (2000)
15. M. Pajda, J. Kudrnovsky, I. Turek, V. Drchal, and P. Bruno: Phys. Rev. Lett. 85, 5424 (2000)
16. O. Grotheer, C. Ederer, and M. Fähnle: Phys. Rev. B 62, 5601 (2000)
17. B. Yaworsky, I. Mertig, A.Y. Perlov, A.N. Yaresko, and V. Antonov: Phys. Rev. B 62, 9586 (2000)
18. P. Kurz, G. Bihlmayer, K. Hirai, and S. Blügel: Phys. Rev. Lett. 86, 1106 (2001)
19. D. Wortmann, S. Heinze, P. Kurz, G. Bihlmayer, and S. Blügel: Phys. Rev. Lett. 86, 4132 (2001)
20. U. von Barth and L. Hedin: J. Phys. C 5, 1629 (1972)
21. K. Knöpfle, L. M. Sandratskii, and J. Kübler: J. Alloys Compd.: 309, 31 (2000)
22. J. Sticht, K.H. Höck, and J. Kübler: J. Phys.: Condens. Matter 1, 8155 (1989)
23. L.M. Sandratskii and J. Kübler: Phys. Rev. B 55, 11395 (1997)
24. L.D. Landau and E.M. Lifshitz: Shape Statistical Physics, Part 1 (Pergamon, New York 1980)
25. J.-C. Tolédano and P. Tolédano: Shape The Landau Theory of Phase Transitions (World Scientific, Singapore 1987)
26. L.M. Sandratskii and J. Kübler: Phys. Rev. B 60, R6961 (1999)
27. L.M. Sandratskii and G. Lander: Phys. Rev. B 63, 134436 (2001)
28. L.M. Sandratskii: Sov. Phys. J. 22 941 (1979)
29. P.H. Dederichs, S. Blügel, R. Zeller, and H. Akai: Phys. Rev. Lett. 53, 2512 (1984)
30. B.L. Györffy, A.J. Pindor, J. Staunton, G.M. Stocks, and H. Winter: J. Phys. F 15, 1337 (1985)
31. Deviation of the propagation vector of the magnetic structure of Cr from 0.5 was not taken into account in early calculations.
32. A. Purwanto, R.A. Robintson, L. Havela, V. Sechovsky, P. Svoboda, H. Nakotte, K. Prokes, F.R. de Boer, A. Seret, J.M. Winand, J. Rebizant, and J.C. Spirlet: Phys. Rev. 50, 6792 (1994)
33. K. Knöpfle and L.M. Sandratskii: Phys. Rev. B 63, 14411 (2001)
34. T. Smith: Phys. Rev. 8, 721 (1916); L. Néel: Rev. Mod. Phys. 25, 58 (1953)
35. I.J. Dzialoshinski: Phys. Chem. Solids 4, 241 (1958)
36. T. Moriya: Phys. Rev. 120, 91 (1960)
37. L.M. Sandratskii, M. Uhl, and J. Kübler: J. Phys.: Condens. Matter 8 983 (1996)
38. F.J. Morin: Phys. Rev. 78, 819 (1950)
39. L. M. Sandratskii and J. Kübler: Europhys. Lett. 33 447 (1996)
40. F.R. de Boer, E. Brück, H. Nakotte, A.V. Andreev, V. Sechovsky, L. Havela, P. Nozar, C.J.M. Denissen, K.H.J. Buschow, B. Vaziri, M. Meissner, H. Malette, and P. Rogl: Physica B 176, 275 (1992)
41. R.A. Robinson, A.C. Lawson, J.W. Lynn, and K.H.J. Buschow: Phys. Rev. B 45, 2939 (1992)
42. R.A. Robinson, A.C. Lawson, J.A. Goldstone, J.W. Lynn, and K.H.J. Buschow: J. Magn. Magn. Mater. 128, 143 (1993)
43. R.A. Robinson, J.W. Lynn, A.C. Lawson, and H. Nakotte: J. Appl. Phys. 75, 6589 (1994)
44. R. Troc, V.H. Tran, M. Kolenda, R. Kruk, K. Latka, A. Szytula, J. Rossat-Mignod, M. Bonnet, and B. Büchner: J. Magn. Magn. Mater. 151, 102 (1995)

45. L.M. Sandratskii and J. Kübler: J. Phys.: Condens. Matter 9, 4897 (1997)
46. S. Tomiyoshi and Y. Yamaguchi: J. Phys. Soc. Jpn. 51, 2478 (1982)
47. B. Ptaciewicz-Bak, A. Baran, W. Suski, and J. Leciejewicz: J. Magn. Magn. Mater. 76–77, 439 (1988); J. Gal, I. Yaar, E. Arbaboff, H. Etedgi, P.J. Litterst, K. Aggarwal, J.A. Pereda, G.M. Kalvius, G. Will, and W. Schäfer: Phys. Rev. B 42, 237 (1989); A.V. Andreev, H. Nakotte, and F.R. de Boer: J. Alloys Compd. 182, 55 (1992)
48. J.A. Paixão, B. Lebech, A.P. Gonçalves, P.J. Brown, G.H. Lander, P. Burlet, and A. Delapalme, J.C. Spirlet: Phys. Rev. B 55, 14370 (1997)
49. S. Demuynck, L.M. Sandratskii, S. Cottenier, J. Meerschaut, and M. Rots: J. Phys.: Condens. Matter 12, 4629 (2000)
50. J.M.D. Coey: Can. J. Phys. 65, 1210 (1987)
51. J. Jensen and A.R. Mackintosh, Rare Earth Magnetism (Clarendon Press, Oxford 1991)
52. O.N. Mryasov, A.I. Liechtenstein, L.M. Sandratskii, and V.A. Gubanov: J. Phys.: Condens. Matter 3, 7683 (1991); M. Uhl, L.M. Sandratskii, and J. Kübler: J. Magn. Magn. Mat. 103, 314 (1992); M. Körling and J. Ergon: Phys. Rev. B 54, 8293 (1996); D.M. Bylander and L. Kleinman: Phys. Rev. B 59, 6278 (1999) and 60, 9916 (1999)
53. K. Knöpfle, L.M. Sandratskii, and J. Kübler: Phys. Rev. B 62, 5564 (2000)
54. L. Nordström and A. Mavromaras: Europhys. Lett. 49, 775 (2000)
55. V. Sechovsky and L. Havela: 'Magnetism of ternary intermetallic compounds of uranium'. In: Handbook of Magnetic Materials, ed. K.H.J. Buschow (Elsevier, Amsterdam 1998) pp. 1–289
56. L.M. Sandratskii and J. Kübler: Mod. Phys. Lett. B 10, 189 (1996)
57. A. Szytula, M. Kolenda, R. Troc, V.H. Tran, M. Bonnet, and J. Rossat-Mignod: Solid State Commun. 81, 481 (1992); R.A. Robinson, A.C. Lawson, J.W. Lynn, and K.H.J. Buschow: Phys. Rev. B 47, 6138 (1993); S. Kawamata, K. Ishimoto, Y. Yamaguchi, and T. Komatsubara: J. Magn. Magn. Mater. 104–107, 51 (1992)
58. D. Mannix, S. Coad, G.H. Lander, J. Rebizant, P.J. Brown, J.A. Paixão, S. Langridge, S. Kawamata, and Y. Yamaguchi: Phys. Rev. B 62, 3801 (2000)
59. O. Nakanishi, A. Yanase, A. Hasegawa, and M. Kataoka: Solid State Commun. 35, 995 (1980)
60. M. Ishida, Y. Endoh, S. Mitsuda, Y. Ishikawa, and M. Tanaka: J. Phys. Soc. Jpn. 54, 2975 (1985)
61. W.C. Koehler: 'Magnetic structure of Rare Earth Metals and Alloys'. In: Magnetic Properties of Rare Earth Metals, ed. R.J. Elliott (Plenum Press, London 1972) pp. 81–128
62. J. Jensen: Acta Phys. Pol. A 91, 89 (1997)
63. B.R. Cooper: 'Phenomenological Theory of Magnetic Ordering: Importance of Interactions with the Crystal Lattice'. In Magnetic Properties of Rare Earth Metals, ed. R.J. Elliott (Plenum Press, London 1972), pp. 17–80
64. A.Y. Perlov, S.V. Halilov, and H. Eschrig: Phys. Rev. 61, 4070 (2000)
65. M.S.S. Brooks, L. Nordström, and B. Johansson: J. Phys.: Condens. Matter 3, 2357 (1991); M. Richter and H. Eschrig: Physica B 172, 85 (1991)
66. L.M. Sandratskii: Phys. Rev. 64, (2001)
67. P. Strange, A. Svane, W.M. Temmerman, Z. Szotek, and H. Winter: Nature 399, 756 (1999)

68. O. Eriksson, B. Johansson, and M.S.S. Brooks: J. Phys. Condens. Matter 1, 4005 (1989)

69. V. Anisimov, J. Zaanen, and O.K. Andersen: Phys. Rev. B 44, 943 (1991); A.I. Liechtenstein, V.P. Antropov, and B.N. Harmon: Phys. Rev. B 49, 10 770 (1994)

70. D.M. Bylander and L. Kleinman: Phys. Rev. B 58, 9207 (1998)

71. H. Eschrig and V.D.P. Servedio: J. Comput. Chem. 20, 23 (1999)

72. M. Todorova, L.M. Sandratskii, and J. Kübler: Phys. Rev. B 63, 52408 (2001)

73. L.M. Sandratskii and J. Kübler: Europhys. Lett. 33, 447 (1996)

74. J. Köhler, L.M. Sandratskii, and J. Kübler: Phys. Rev. B 55, R10153 (1997)

75. W. Reim and J. Schoenes: 'Magneto-optical Spectroscopy of f-electron Systems'. In: Ferromagnetic Materials, Vol. 5, eds. K.H.J. Buschow, E.P. Wohlfarth (North-Holland, Amsterdam 1990) pp. 133–236

76. Metallic Magnetism. ed. by H. Capellmann (Springer, Berlin Heidelberg New York 1987)

77. H. Ebert, J. Minar, V. Popescu, L.M. Sandratskii, and A. Mavromaras: AIP Conf. Proc. 514, 110 (2000)

Springer Series in
## MATERIALS SCIENCE

D.J. Singh
D.A. Papaconstantopoulos
(Eds.)

# Electronic Structure and Magnetism of Complex Materials

With 159 Figures

Springer

Dr. David J. Singh
Dr. Dimitrios A. Papaconstantopoulos
Code 6391, Naval Research Laboratory
Washington, DC 20375, USA
E-mail: sing@dave.nrl.navy.mil
        papacon@dave.nrl.navy.mil

Springer Series in
# MATERIALS SCIENCE 54

Springer
*Berlin*
*Heidelberg*
*New York*
*Hong Kong*
*London*
*Milan*
*Paris*
*Tokyo*

**Physics and Astronomy**   ONLINE LIBRARY

http://www.springer.de/phys/